A 60–50 ka African Humid Period modulated by stadial Heinrich events HE6 and HE5a in northwestern Africa

A. Nutz, O. Kwiecien, J.P. Buylaert, Abel Guihou, I. Khabouchi, P. Deschamps, S.F.M. Breitenbach, P. Poirier, Pierre Dietrich, L. Kabiri, et al.

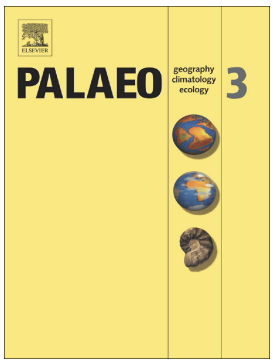

A 60–50 ka African Humid Period modulated by stadial Heinrich events HE6 and HE5a in northwestern Africa

A. Nutz, O. Kwiecien, J.P. Buylaert, A. Guihou, I. Khabouchi, P. Deschamps, S.F.M. Breitenbach, P. Poirier, P. Dietrich, L. Kabiri, B. Essafraoui, S. Bodin

PII: S0031-0182(23)00570-9

DOI: https://doi.org/10.1016/j.palaeo.2023.111952

Reference: PALAEO 111952

To appear in: *Palaeogeography, Palaeoclimatology, Palaeoecology*

Received date: 17 May 2023

Revised date: 4 October 2023

Accepted date: 28 November 2023

Please cite this article as: A. Nutz, O. Kwiecien, J.P. Buylaert, et al., A 60–50 ka African Humid Period modulated by stadial Heinrich events HE6 and HE5a in northwestern Africa, *Palaeogeography, Palaeoclimatology, Palaeoecology* (2023), https://doi.org/10.1016/j.palaeo.2023.111952

A 60-50 ka African Humid Period modulated by stadial Heinrich events HE6 and HE5a in northwestern Africa

A. Nutz[1], O. Kwiecien[2], J.P. Buylaert[3], A. Guihou[1], I. Khabouchi[1], P. Deschamps[1], S.F.M. Breitenbach[2], P. Poirier[1], P. Dietrich[4], L. Kabiri[5], B. Essafraoui[5], S. Bodin[6]

[1]*Aix Marseille Univ., CNRS, IRD, INRAE, Coll. France, CEREGE, Europôle Méditerranée de l'Arbois BP 80 13545 Aix-en-Provence, cedex 4, France*

[2]*Department of Geography and Environmental Sciences, Northumbria University, Newcastle upon Tyne, UK.*

[3]*Department of Physics, Technical University of Denmark, DTU Risø campus, Roskilde, Denmark.*

[4]*Univ Rennes, CNRS, Géosciences Rennes, UMR 6118, 35000 Rennes, France*

[5]*Département de Géologie, Faculty of Science and Technology of Errachidia (FSTE), Université Moulay Ismail (UMI), Errachidia, Morocco.*

[6]*Department for Geoscience, Aarhus University, Aarhus, Denmark.*

Keywords

Paleolake, African Humid Period, Human dispersal, Morocco, Late Pleistocene

Abstract

A Late Pleistocene lacustrine sedimentary succession has recently been discovered and investigated in Northwest Africa (Morocco, Anti-Atlas, Agadir-Tissint Feija). By integrating new radiometric ^{230}Th/U and OSL ages and new clay mineral analyses with previous sedimentological evidence, we significantly refine the origin and the timing of this succession and its significance for African paleoenvironments and paleoclimate. The sedimentary succession reflects the evolution of a paleolake, referred to as paleolake Tissint, that indicates the abrupt establishment of a wet period at ~60 ka and a gradual return to drier conditions at ~50 ka. Establishment of this paleolake coincides with a peak of precession-forced high summer insolation centered around ~60 ka suggesting that orbital parameters triggered humid conditions in northwest Africa during this time interval. Comparing this observation with others from the literature, it appears that continental-scale wet conditions prevailed across North, Central and East Africa at that time and add evidence in support of a 60-50 ka African Humid Period (AHP). Given that the Holocene African Humid Period was associated with "Green Sahara" conditions, wet conditions between 60 and 50 ka likely sustained coeval greening, at least partially, of the Sahara region. In northwest Africa, the 60-50 ka AHP is affected by Heinrich Event HE6 which via adjustment of the Atlantic Meridional Ocean Circulation (AMOC) seems to have delayed the onset of this AHP. In a similar way, the younger Heinrich Event 5a resulted in short-term regional aridification about 55 ka ago that briefly interrupted the generally wetter period. Finally, as the AHP between ~60 ka and ~50 ka coincides with a major Human dispersal out of Africa; these particular conditions may have

offered a climatic window of opportunity for *Homo sapiens* to open migration routes across Africa towards the Levant.

1. Introduction

Since the Miocene, more than 230 wet periods, referred to as African Humid Periods (AHPs), resulted in episodes during which savannah expanded, drainage developed and lakes established across most of North, Central and East Africa including the Saharan desert (e.g., Larrasoana et al., 2013). These wet periods are understood to have constituted key time windows for faunal and human evolution and dispersal through the establishment of corridors that connected individual hydrographic basins, which were mostly isolated during drier periods (e.g., Drake et al., 2022). AHPs were triggered by increasing insolation related to changes in precessional orbital parameters of the Earth (deMenocal et al., 2000). These cyclical insolation changes paced African monsoon intensity, notably by adjusting the amplitude of the seasonal northward shift of the Intertropical Convergence Zone (ITCZ), and winter rain in the Mediterranean Basin (Kutzbach et al., 2020). In response, countless wetlands and lakes developed or extended in both, Central (Schuster et al., 2005; Drake et al., 2008, 2022) and Eastern Africa (Ashley 2007, Garcin et al., 2012; Junginger and Trauth, 2013; Nutz and Schuster, 2016; Nutz et al., 2017, 2020) during periods of high summer insolation. During the last glacial cycle, AHPs were recognized only during interglacial periods, between 128-124 ka, 81-77 ka and 11-5 ka (de Menocal et al., 2000; Bard, 2013; Larrasoana et al., 2013; Shanahan et al., 2015). Between the two last AHPs (i.e., the interval between ca. 77 and 11 ka), persistently drier conditions without significant wet intervals are postulated in Africa, coeval with the last glacial phase (e.g., Tjallingii et al., 2008; Grant et al., 2017).

In northwestern Africa, the overlapping effects of Atlantic and Western Mediterranean air masses, superimposed on the influence of the African monsoon add significant complexity to the climate configuration (Kuhlmann et al., 2004; Tierney et al., 2017a; Zielhofer et al., 2017, 2019). In this context, some important aspects remain poorly known; first, the northern maximum expansion of the West African monsoon is still debated for the last AHP (Tierney et al., 2017a), and remains unknown for earlier ones; second, the potential impact of both glacial-interglacial cycles and dynamics of the northern hemisphere ice sheet remain only indirectly envisioned (Kinsley et al., 2021, Aït Brahim et al., 2023) and third, although a potential effect of millennial to centennial-scale cycles in Atlantic Ocean dynamics on African climate has been suggested for the Holocene (Olsen et al., 2012; Wassenburg et al, 2013; Zielhofer et al., 2017, 2019), no evidence has so far been presented for earlier periods.

Here, we investigate the recently described Late Pleistocene sediments of the Agadir Tissint Feija (Nutz et al., 2019) in greater detail and combine new radiometric dates and clay mineralogy analyses to identify and chronologically constrain a previously unobserved

African wet period between 60 and 50 ka, coeval to a precession minimum during the last glacial phase. In addition, we discriminate different second-order climatic forcings in northwest Africa during the Late Quaternary. Finally, our findings highlight the complexity of climate dynamics in this region; an area that is increasingly affected by current climate change (Giorgi, 2006; Diffenbaugh and Giorgi, 2012).

2. Geological setting

Between the southern front of the Anti-Atlas (Morocco) and the escarpment of the Jbel Bani, rivers draining the relief form narrow valleys and feed extensive 15–50 km wide lowlands locally called 'Feijas' (Fig.1A). There are five major Feijas in southern Morocco, one of which is the Agadir-Tissint Feija. It is *ca.* 20 km long and *ca.* 7 km wide, representing a *ca.* 120 km² feija located between 29.8°N and 30°N, linked to a catchment area of >3,200 km^2 (Fig. 1B). Downstream the feija, the Jbel Bani is crossed by the Tissint river in a gorge that constitutes the modern outlet of the system (Fig. 1C).

In the Agadir-Tissint Feija (Anti-Atlas, Morocco), a Late Pleistocene sedimentary succession has recently been discovered and investigated (Fig. 1D and 2A; Nutz et al., 2019). The authors combined information from four sectors to depict the basin-scale architecture of this depocentre. Overlying a fluvial carbonate tufa interpreted as ancient carbonate-rich fluvial system (Fig. 2B and C), the studied succession reveals 12 m-thick lacustrine deposits (Figs. 2A and 3) that evidence the existence of a paleolake, referred to as paleolake Tissint. This lake was characterized by low-energy sedimentation of clastic- or calci-mud (Fig. 2D and E). Low-energy vegetated margins and shores encircled this lake (Fig. 2F and G), except where rivers entered and sandy river mouth complexes developed. The estimated locations of the paleoshorelines suggest that paleolake Tissint covered an area of, at most, ca. 10 km², laterally associated with a vegetated fluvial floodplain. Downstream, paleolake Tissint was blocked by a carbonate tufa dam build in the Tissint Gorge. Carbonate tufa dams result from degassing of CO_2 in agitated waters with high velocity and turbulence. Several authors (Arenas et al., 2010, 2015; Auqué et al., 2014 ; Sancho et al., 2015 among others) depicted a direct positive correlation between water supply and tufa precipitation, which makes tufa dams development as a proxy for wetter periods. Azennoud et al. (2022) recently comforted this correlation showing that during the last 5 ka humid periods led to the aggradation of tufa dams and lake developments in central Morocco (region of Immouzzer Kandar). Similarly, pulses of tufa dam construction in the Tissint gorge directly derived from more humid periods associated with increased water supply due to increased precipitation in the paleolake Tissint catchment (Nutz et al., 2019). Following, the progressive disappearance of paleolake Tissint indicates an interruption of tufa dam aggradation in the Tissint gorge and the return to drier conditions. Then, the Agadir-Tissint Feija was dominated by sedimentation of coarser-grained

material and was occupied by several tens of metres wide river channels that were laterally associated with overbank deposits (Fig. 2A).

3. Materials and methods

3.1. Chronology

In addition to two previously dated layers (L1 and L8) described in Nutz et al. (2019) and Thorp et al., (2002), respectively, three additional layers were newly dated. Layer L3 has been dating using ^{230}Th/U, and layers L6 and L7 were dated using Optically Stimulated Luminescence (OSL). In total, eight layers (L1-L8, with L1 being the oldest, Table 1) distributed along the type section (Figs. 1D, 2A, 3) are now directly dated, or their age has indirectly been estimated using sedimentation rates in uniform lithologies, to provide a new chronological framework for the Agadir Tissint Feija (Fig. 3). The numerical dates are summarized in Table 1, with their locations given Figs. 2A and 3.

The age of L1 was obtained using the ^{230}Th/U dating method applied to phytoherm boundstones of stems. It is estimated at 69.45±0.3 ka (Nutz et al., 2019). This age agrees well with two stratigraphically lower samples that are situated a few centimetres below L1 (W53-U1 & U3; Table 1) showing slightly older ages.

The age of layer L3, based on sample TISS-20-08 collected in phytoherm boundstones of stems, is added in the present study. The geochronological analysis was carried out at CEREGE laboratory. Due to the generally relatively large amount of initial detrital Th in sediments of the Agadir Tissint Feija, the three-dimensional isochron method was used as a more reliable approach for this type of samples (Ludwig and Titterington, 1994). Five aliquots of sample TISS-20-08 were prepared within two batches (2 aliquots in 2020 and 3 in 2021) and spiked with a mixture of ^{229}Th-^{233}U-^{236}U following the method described in Weil-Accardo et al. (2022). Analyses were carried out using a Neptune+ MC-ICP-MS. Procedural blanks were <5 fg for ^{234}U, <30 pg for ^{238}U, <5 fg for ^{230}Th and <60 pg for ^{232}Th. The (^{230}Th/^{238}U) ratios of preparations of the HU-1 uraninite standard were 1.003±0.005 in 2020 and 1.004±0.002 in 2021 in agreement with the accepted value (Cheng et al., 2013). Results on the 5 aliquots show good overall consistency and provide a calculated three-dimensional isochron age of 55.4±3.5 (based on the Maximum Likelihood Estimation of IsoplotR; Vermeesch, 2018; Fig. S1). The uncertainty arises from the expansion using the high MSWD = 60 which likely results from a large geological scatter linked to high variability in the detrital end-member. The calculation of the initial (^{230}Th/^{232}Th) of the detrital endmember based on the three-dimensional isochron is 0.9±0.1, in agreement with the bulk Earth ratio of 0.8±0.4, which provides robustness to the isochron age of sample TISS-20-08.

The ages of layers L6 and L7 are based on the OSL method carried at the Copenhagen laboratory. L6 and L7 were collected in fluvial sandstones. Sample tubes used for luminescence sampling were opened in subdued orange light (Sohbati et al., 2017) to avoid

signal loss during sample preparation. Approximately 170 g of outer tube material was used for dose rate analysis using high resolution gamma spectrometry (Murray et al., 2018). One portion of the inner material was wet-sieved to isolate 180-250 µm grains and this fraction was first treated with 10% HCl and 10% H_2O_2. The samples were washed at least 3 times with deionised water after each acid treatment. The grains were then immersed in a 10% HF solution for 40 mins to remove oxide coatings from the grains and to remove the outer alpha-irradiated layer from the K-feldspar grains. K-rich feldspar grains were separated from the heavier quartz grains using a 2.58 g/ml heavy liquid solution (LST Fastfloat^{TM}). The quartz grains were then etched again using concentrated HF for 1 hour. After each HF treatment the grains were washed in 10% HCl to avoid precipitation of CaF2. Another portion of the inner tube material was used to determine the 'in situ' present day water content and to determine the saturation water content using the syringe method (Murray et al., 2021). Extracted quartz grains were mounted as large aliquots on stainless steel discs and K-rich feldspar grains as 2 mm diameter aliquots in stainless steel cups using silicon oil as an adhesive. All measurements were made using Risø TL/OSL readers model DA-20 (Bøtter-Jensen et al., 2010) equipped with blue and IR diodes. For blue-light stimulated quartz OSL signals the initial 0.8s of the signal minus the subsequent 0.8 s was used for calculations; preheat and cut-heat settings were 260°C/10 s and 220°C, respectively. For K-rich feldspars, the initial 2 s of the IRSL decay curve minus the last 20 s was used for calculation. Quartz OSL measurements were made using a double-SAR protocol (Banerjee et al., 2001) because we found a significant IRSL response from the quartz-rich extract. The post-IR blue signal from quartz is dominated by a fast component but for all three samples the natural signal lies close to or is in saturation on the dose response curve (data not shown). Therefore, the quartz OSL signal was not considered further to date these samples. Feldspar was measured using a $pIRIR_{200,290}$ protocol (e.g., Li and Li, 2012; Stevens et al., 2018) which has been shown to not require fading correction. The hard-to-bleach component of the $pIRIR_{200,290}$ signal was estimated by bleaching 3 aliquots per sample under a Hönle Sol2 solar simulator. The measured residual dose is 14.8±0.5. Gy which was subtracted from all measured D_e values prior to age calculation. The analytical results and ages are presented in Table 1. Finally, samples collected in layer L6 indicate ages of 46.2±2.1 ka and 42.9±2 ka and reveal a mean age of 44.6±1.8 ka while the age of layer L7 is based on a single sample dated to 34.4±1.4 ka.

Subsequently, sedimentation rates were estimated based on the dated layers L3, L6, L7 and L8 (Fig. 3; Table 1) and extrapolated to adjacent portions of sections with comparable lithologies. Based on ages of layers L6 and L7, a mean sedimentation rate of 0.4 m/ka is applied in the lower part of the fluvial sandstones to extrapolate the age of L5 that is now estimated around ~50 ka (Fig. 3). A sedimentation rate of 0.3 m/ka in the upper part of the fluvial sandstones, between L7 and L8, reveals a relative constant mean sedimentation rate in fluvial sandstones (Fig. 3). Approximating a mean sedimentation rate of 1.5 m/ka in lacustrine

deposits between layers L3 and L5, we estimated the ages of L2 and L4 at ~59 ka and ~55 ka, respectively. In Nutz et al. (2019), an additional interval was dated with a single sample (Ti_S1_014; Table 1) collected around 3.5 m below L3, in calci-mud. Showing a younger age than the isochron-based age of L3 located above, we excluded this age from our newly refined chronological framework.

3.2. Clay mineralogy

A total of 21 samples, collected along the type section (Figs. 2A, 3B), were analysed for their mineralogy using X–ray diffraction (XRD). Eleven samples were processed at the Department of Geoscience, Aarhus University, Denmark, and 10 samples were analysed at the CEREGE laboratory, Aix-Marseille University, France. In both laboratories, analyses were performed on oriented mounts of decarbonated clay-sized particles (<2 μm). For each sample, three XRD runs were carried out after air–drying, ethylene–glycol solvation and heating to 500°C for one hour. In both laboratories, a PANalytical X'Pert Pro MPD instrument was used. Proportions of smectite, illite, kaolinite, and chlorite were estimated for each sample based on diffractogram analyses. Estimates of clay mineral abundances are based on the integrated peak areas of the individual peaks and weighting factors.

Smectite (S) and kaolinite (K) minerals result from moderate to intense chemical weathering (Chamley, 1989). In contrast, illite (I) and chlorite (Cl) are considered to be products of physical disaggregation, or moderate chemical alteration of feldspar and mica (Chamley, 1989). In parallel, recent studies suggested that evaporation-forced increased alkalinity and/or salinity may foster low-temperature illitisation of smectite (Foerster et al., 2018; Schaëbitz et al., 2021). Thus, we consider smectite and kaolinite are likely to form in soils affected by significant chemical weathering in warm and humid conditions, while illite and chlorite are derived from lower-intensity chemical weathering or physical erosion of bedrock in cooler and drier conditions (Chamley, 1989) or illitisation of smectite during drier intervals. Consequently, the (S+K)/(I+Cl) ratio is a valuable proxy for the relative intensity of (wet) chemical or (dry) physical weathering used as a robust indicator for weathering intensity in the paleolake catchment and for increased evaporation.

4. Results

Building upon new dating, clay mineralogy and previous sedimentological observations, we are now able to detail the evolution and timing of paleoenvironmental changes in the Agadir Tissint Feija including paleolake Tissint establishment, fluctuations and disappearance.

Fluvial tufa of the lowermost part of the succession is direct evidence of a relative dry period, probably comparable to present-day, when perennial rivers drained the Agadir Tissint Feija (Fig. 3A). Dating reveals that this fluvial system was active for at least 5,000 years, between ~75.10±0.3 ka and ~69.75±0.2 ka (Nutz et al., 2019). After ~69.75±0.2 ka, according

to the estimated age of layer L2, we suspect a ~10 kyr long non-depositional period in the central portion of the Agadir Tissint Feija before paleolake Tissint flooded the area (Fig. 3A). During that period, development of the fluvial tufa interrupted likely in response to reduced riverine water flows due to slightly drier conditions in the depocentre. On the contrary, the subsequent transition to a lacustrine environment, estimated to have occurred at ~59 ka, provides clear evidence for wetter conditions in the region. The sediment succession of paleolake Tissint starts with a ~5 m thick deposit of muds (interval S1 according to Nutz et al., 2019; Fig. 2A and 3) revealing perennial lacustrine conditions. Interval S1 is topped by a m-scale interval of carbonate tufa mostly composed of phytoherm boundstones (Fig. 2F and G). This tufa is evidence of a shallow lake margin laterally associated with paludal shores (Fig. 3B) indicating a short-term aridification estimated around ~55 ka (Fig. 3). Sequence S1 is overlain by a second ~6 m thick mud interval (S2 according to Nutz et al., 2019; Fig. 2A) which suggests renewed perennially lacustrine conditions. Upward, the lacustrine muds are overlain by ~13 m thick fluvial sandstones indicating that paleolake Tissint disappeared due to the return of progressively drier conditions; this aridification occurred at ~50 ka (Fig. 3E). It worth noticing that the aforementioned chronology of paleolake Tissint evolution significantly differs from the chronology proposed by Nutz et al., (2019). In this pioneer study, the lacustrine interval was tentatively estimated between 69 ka and 20 ka; new ages for L3, L5 and L6 layers now discard such interpretation. Superimposed on this long-term lacustrine interval that spans S1 and S2 are 51 alternations of dm-scale carbonate and clastic mud beds. Of these, 26 alternations are in sequence S1 and 25 in sequence S2. Expressing the repetitions of open and endoreic lacustrine conditions (Nutz et al., 2019), these alternations reveal high-frequency fluctuations of the paleolake level that mirror successive short-term arid and humid periods, respectively. Even if the radiometric age uncertainties do not allow to accurately estimate their periodicity, these alternations represent submillennial cycles of significant paleohydrological changes.

Clay mineralogy analyses of the lacustrine deposits show that smectite and illite dominate throughout the type section (Fig. 3) while kaolinite and chlorite are found subordinate. From base to top, smectite dominates with maximum values of 75% of all clay minerals in the lowermost part of the succession, but progressively diminishes to 25% in the upper part. Illite is anticorrelated to smectite, representing 25% of the clay mineral assemblage in the lower part of the succession, and grading to 70% in the upper part. Thus, clay mineral ratios testify intense chemical weathering in paleolake Tissint catchment coeval with the lowermost part of the lacustrine succession and a subsequent progressive reduction of the weathering intensity and/or the replacement by increasing mechanical disaggregation. Additionally, if we consider a proportion of illite abundance derived from low-temperature illitisation of smectite, this suggests a coeval progressive increase of alkalinity due to increasing evaporation. Thus, the replacement of smectite with illite reflects progressive

regional aridification. The wettest conditions occurred shortly after the establishment of paleolake Tissint, followed by a progressive aridification throughout the evolution of the paleolake. Clay mineralogy shows a single humid phase that reached its maximum shortly after ~60 ka and successively shifted towards drier conditions until ~50 ka. Interestingly, the evolution of the clay mineralogy seems to be independent of the intense arid episode estimated at ~55 ka. This suggests that this short-term aridification did either not persist long enough to modify weathering processes in the catchment area or did not affect the Anti-Atlas relief and was focused only the Agadir Tissint Feija lowland.

5. Climatic implications

5.1. A 60-50 ka African Humid Period

New chronological constraints of paleolake Tissint reveal a humid period in the Agadir Tissint Feija that occurred shortly after ~60 ka and lasted until ~50 ka. Clay mineral analyses indicate that weathering intensity in the catchment of the Agadir Tissint Feija closely responded to this humid period, with a maximum estimated shortly after ~60 ka. The peak of this humid period is coeval with a maximum in summer insolation at ~60 ka, and subsequent progressive aridification coincides with decreasing summer insolation from ~60 to ~50 ka (Fig. 3). In this context, the establishment of wetter conditions in the Agadir Tissint Feija is attributed to the intensification of the West African monsoon. Precession-forced insolation increase pushed northward the influence of the ITCZ increasing rainfall; a traditional origin for successive AHPs since the Miocene (Larrasoaña et al., 2013). In previous publications, some authors invoked an influence of the West African monsoon up to 31°N during the Holocene AHP (Tierney et al., 2017a; Sha et al., 2019) comforting the potential influence of the West African monsoon in the Agadir Tissint Feija. Here, we suggest a similar configuration during the 60-50 ka period. Alternatively, no precipitation increase is reported between 60 and 50 ka in the Mediterranean realm (Wagner et al., 2019). This suggests a relative minor contribution of humidity from the Mediterranean region. Moreover, the location of the Agadir Tissint Feija southeastward the SW-NE oriented High-Atlas and Anti-Atlas ranges likely limits the potential impact of both Mediterranean air masses and westerlies as precipitation providers due to orographic effects.

Even with limited data currently available for the 60-50 ka interval in most African catchments that experienced more humid environments or hosted paleolakes during some Quaternary African Humid Periods (i.e., Ahnet-Mouydir, Chad, Chew Bahir, Chott, Congo, Darfur, Draa, Fezzan, Niger, Nile, Timbuktu, Turkana, Tushka), wetter conditions seem to be observed at that time in multiple areas across Africa where records exist. Here we present a compilation of paleohydrological conditions for the 60-50 ka time interval at different locations in Africa (Fig. 4). Direct evidence of wetter conditions at ~60 ka is recorded in the

Dakhla oasis with the deposition of the "Pleistocene Lacustrine sediments" revealing a lake developed at that time (Brooke, 1993) and wet conditions in northeast Africa. Meanwhile, humidification of northwest Africa between ~60 and ~50 ka was recently proposed by Kinsley et al. (2021) based on indirect evidence (i.e., dust concentration) in a marine core from the Atlantic (Fig. 4B). These authors show that dust flux broadly decreased from ~60 to ~50 likely indicating vegetation development onshore, in the western Saharan domain, except during a brief episode centred around ~55 ka during which dust flux drastically increased likely originated from a short-term vegetation reduction. A decrease in Total Organic Carbon (Fig. 4B) comparable with the decrease observed during the last AHP in deposits of the Congo deep sea fan (Dalibard et al., 2014) suggests reduced marine productivity during the 60-50 ka interval. Moreover, the Ba/Ca ratios in that core suggest lower salinity offshore the Congo River mouth (Fig. 4B) which the authors attribute to increased freshwater supply in response to stronger West African monsoon intensity and more abundant rainfall in the Congo catchment. Similarly, evidence for reduced salinity in the Niger River delta (Fig. 4B) between ~60 and ~50 ka supports increased freshwater runoff from the Niger catchment and wetter conditions in the Sahel region (Weldeab et al., 2007). In the Nile delta, higher Fe abundance during the 60-50 ka interval (Revel et al., 2010; Ehrmann et al., 2016; Fig. 4B) suggests higher discharge linked to wetter conditions in the Nile catchment. More recently, Schaëbitz et al. (2021) and Foerster et al., (2022) suggested wetter conditions in the Chew Bahir basin (Ethiopia, East Africa) between ~63 and ~59 ka and around ~60 ka, respectively. Although this wetter period is shorter and slightly earlier to the 60-50 ka AHP, it coincides with the insolation maximum and likely indicates a rapid response of rainfall and the establishment of a short-term precession-driven humid period in this part of East-Africa. By contrast, δD in core RC09-166 in the Gulf of Aden, northeast Africa (Tierney et al., 2017b), reveals drier conditions at around 60 ka. However, a rapid transition to wetter conditions observed between ~58 and ~48 ka would be in line with our inferred 60-50 AHP interval, possibly with a 2-3 ka lag. Thus, even if data for the considered time interval are scarce, direct evidence of a more humid period in northwest Africa and indirect indications of humidification in different African basins, including the three largest catchments of Africa (i.e., Nile, Congo, and Niger rivers catchments), support a previously unrecognized continental-scale African Humid Period between ~60 and ~50 ka. AHPs are commonly presumed to occur during interglacial phases and inhibited during glacial phases as cooling due to enhanced ice-sheet albedo limits their amplitude. The 60-50 ka AHP indicates that wetter conditions have nevertheless established during a glacial phase and these wet conditions were intense enough to allow the development of significant lakes together with increased vegetation cover. As a consequence, we propose that associated environmental changes may have offered favourable conditions for faunal expansion, including *Homo sapiens*, over north, central, and east Africa and thus promoted dispersal out of Africa by opening inland migration routes. Such inland humid

corridors may have provided the environmental context for the latest major dispersal event of *Homo sapiens* out of Africa around 60 ka (Groucutt et al., 2015; Galway-Witham et al., 2019; Bergström et al., 2021).

5.2. Influence of the NH ice sheet in northwest Africa

In the Agadir Tissint Feija, the seemingly early climax of the 60-50 ka humid period suggests the absence of progressive humidification with increasing insolation between ~65 and ~60 ka. Interestingly, this configuration mirrors the onset of the last AHP (11-5 ka), during which, at comparable latitudes (i.e., 30°N), the AHP onset was abrupt and broadly coeval with the peak of insolation (Tierney et al., 2017a). Menviel et al. (2021) recently suggested a similar delay for the 128-124 ka centered AHP. Based on modelling, these authors propose that Heinrich Event (HE) stadials (Heinrich, 1988) can delay the response of rainfall to increased insolation by weakening the AMOC as a response to a freshwater pulse in the polar north Atlantic, thereby limiting the northward migration of the ITCZ. In this case, the respective onsets of the 128-124 and 11-5 AHPs would be controlled by AMOC strengthening at the end of stadials, which in these cases coincide with peak insolation, leading to a rapid increase of rainfall. In the Agadir Tissint Feija, the estimated onset of the paleolake Tissint (~59 ka) slightly lags HE6, ending at around 60 ka (Channell et al., 2012). Thus, our results support the proposed impact of AMOC dynamics related to stadial HE6 on the onset of the 60-50 ka centered AHP. Subsequently, the 60-50 ka AHP is interrupted in the Agadir Tissint Feija by a short-term aridification period recorded by an abrupt shallowing of paleolake Tissint until partial emersion. Considering the estimated age of this interval (~55 ka), it is important to note that it coincides with stadial HE5a. Short-term aridification during this stadial is also indirectly observed along the western African margin and sediments of the Nile Delta (Fig. 4B). Recently, Ait Brahim et al. (2022) observed a similar configuration in northwest Africa for HE1, HE7a, HE7b and HE8.. Recently, Zielhofer et al., 2017 demonstrated that during early Holocene, winter precipitation decreased in northwest Africa during periods of increased meltwater discharge from the NH ice sheet (i.e., equivalent to Heinrich Events). Even if no information exists prior the Holocene, this relationship is envisaged for pre-Holocene periods to support observed aridification during Heinrich event HE5a. In parallel, summer precipitation also decreases during these particular periods of high meltwater discharge into the North Atlantic Ocean in response to weakened AMOC (Menviel et al., 2021). Weakened AMOC leads to reduced SST in the North Atlantic Ocean and as a consequence limits the northward shift of the ITCZ. Finally, it seems that during HE, both summer and winter precipitation were reduced.

6. Conclusions

New ^{230}Th/U and OSL ages and clay mineral analyses, together with geological investigations allow us to refine the origin and timing of Paleolake Tissint. We discuss the significance of this lacustrine succession for African paleoclimate. In the Agadir Tissint Feija, northwest

Africa, a wet period started at ~60 ka and ended ~50 ka, coeval with a precession-forced summer insolation peak. Compiling field-based observations with evidence across Africa from the literature, we propose that this wet period is observed in North, Central, and East Africa and constitutes a previously unknown 60-50 ka humid period likely coeval with continental-scale greening during the last Glacial phase. This wet period may have opened dispersal corridors that facilitated *H. sapiens* migrations across and out of Africa during the 60 ka dispersal event. Greening of the Agadir Tissint Feija during this interval confirms the potential action of the African monsoon up to 30°N latitude during periods of high insolation and wetter climate in northwest Africa even during glacial phases. At the same time, stadials HE6 and HE5a delayed the onset of, or interspersed the 60-50 ka centered AHP in northwest Africa, through their impacts on the AMOC. As such, we confirm the fundamental influence of the northern hemisphere ice sheet dynamics on northwest Africa paleoclimate for periods prior to the Holocene. Finally, we also identified significant submillenial paleohydrological changes before the Holocene in northeast Africa even if they remain to be precisely characterized. The Agadir Tissint Feija provides a particularly valuable archive for understanding local to regional responses of terrestrial systems to global climatic processes. This study also highlights the importance of considering regional terrestrial archives as an essential complement to long-term marine cores.

Acknowledgements

This work is a contribution to the FAGTI project (A. Nutz) funded by CNRS INSU SYSTER action. S. Bodin thanks the Faculty of Science and Technology of Aarhus University for a 2016 starting grant, which was instrumental in initiating this research project. CEREGE has received fundings from 2 french « Investissement d'avenir » program: the EQUIPEX ASTER-CEREGE and the DATCARB project from the « Excellence Initiative » program of Aix Marseille University A*MIDEX. M. Defrance and H. Mariot are thanked for their careful maintenance of the clean lab at CEREGE.

Figures

Fig. 1. Locations maps and photograph. A) Digital elevation model of southwestern Morocco showing the Anti-Atlas and its surrounding areas. Location of the Agadir Tissint Feija is indicated by the red rectangle (modified after Nutz et al., 2019). Topographic profiles reveal that feijas constitute the first lowlands south of the Anti-Atlas. B) Digital elevation model of the Agadir-Tissint Feija catchment. The main rivers draining the area are shown together with the catchment area of the Tissint depocentre. C) Satellite image (Google Earth, 2016) showing the studied depocentre and the location of the type section. D) Photographic panorama of the Agadir Tissint Feija with the location of the type section.

Fig. 2. Field photographs and close-up views on facies observed in the type-section. A) Photographic panorama of the central portion of the Agadir Tissint Feija with the type section. Lacustine sequences S1 and S2 are overlain by fluvial sandstones. Datum layers (L1-L8) are located on the exposure. B and C) Successive cascades and pools forming a stepped fluvial tufa system. This system was subsequently flooded by paleolake Tissint. D and E) Lacustrine deposits made of clastic muds (D) or alternations of clastic and calci-muds (E). F and G) Paludal lake shore deposits made of phytoherm boundstones (F) and showing moulds of vertical stems (G). These deposits are intercalated between S1 and S2 and mark an important lake shallowing and partial emersion phase between the two lacustrine intervals S1 and S2. See Nutz et al. (2019) for detailed facies interpretations.

Fig. 3. Summary of sedimentary data, chronological constraints and inferred palaeoclimate evolution for the ~75-10 ka time interval. Successive sedimentary systems are presented through time (see details in Nutz et al., 2019) and the type-section is shown with locations of dated layers. Comparison with the insolation curve (Laskar et al., 2004) shows that paleolake Tissint coincides with a high insolation period at 60 ka, initiating just after the HE6 stadial and interspersed by stadial HE5a.

Fig. 4. A) Map showing the main African hydrographic catchments and their hydrological conditions at ~60 ka. AG, Aden Gulf; AMB, Ahnet Mouydir Basin; ATF, Agadir Tissint Feija; BC, Bosumtwi crater; CB, Chotts Basin; CBB, Chew Bahir Basin; ChB, Chad Basin; ConD, Congo river delta; NiD, Niger river delta; NileD, Nile river delta; DO, Dakhla Oasis; FB, Fezzan Basin; TB, Timbuktu Basin; TM, Tamanrasset paleoriver mouth; TurB, Turkana Basin. B) Compilation of humidity proxies for different locations of Africa (location. Fig. 4A). From left to right, dust concentration in core ODP658C (Kinsley et al., 2021). TOC in the Congo deep sea fan and Ba/Ca ratios in the Congo and Niger deltas as marker of productivity and salinity changes, respectively (Weldeab et al., 2007; Dalibard et al., 2014). Fe abundance in the Nile delta as a proxy of the Nile River discharge (Ehrmann et al., 2016). K abundance in lacustrine sediments of the Chew Bahir basin (Schaëbitz et al., 2021) as proxy of increase alkalinity and salinity and by extension of lake level. δD in core RC09-166 of the Gulf of Aden (Tierney et al., 2017b) showing indication of rainfall intensity. Altogether, proxies provide evidence for wetter conditions associated with the 60 ka centered peak of insolation and suggest the establishment of an African Humid Period between 60 and 50 ka.

Table 1. Compilation of ^{230}Th/U and OSL ages used to date the L1 to L8 layers along the type section. The new ^{230}Th/U age of L3 is based on a three-dimensional isochron calculated by IsoplotR (Vermeesch, 2018) in the (^{238}U/^{232}Th) – (^{230}Th/^{232}Th) space, also called Rosholt (Ludwig and Titterington, 1994). Regression uses a Maximum Likelihood estimation. Half live values are given in Cheng et al. (2013). Concerning OSL dating of L6 and L7, burial depth below topographic surface, water content (w.c.), radionuclide concentrations, total dose

rate to 180-250 µm K-feldspar grains, equivalent dose, number of aliquots (n) and $pIRIR_{200,290}$ age are indicated. Radionuclide concentrations were converted to beta and gamma dose rate components using the conversion factors from Guérin et al. (2011). All uncertainties are given at 1 standard error. The $pIRIR_{200, 290}$ are not corrected from instability (e.g., Buylaert et al., 2012).

Fig. S1. ^{230}Th-U isochron diagram of sample TISS-20-08. Results for the 5 analyzed aliquots are plotted in the (^{238}U/^{232}Th) vs (^{230}Th/^{232}Th) "Rosholt" space with IsoplotR (Vermeesch, 2018) using the maximum likelihood estimation for regression. Uncertainty of the isochron age is given at the 95% confidence interval level (left) and expanded by the MSWD (right). 2σ error ellipsoids are shown for each aliquot. The calculated initial (^{230}Th/^{232}Th) is also provided.

References

Ait Brahim, Y., Sha, L., Wassenburg, J.A., Azennoud, K., Cheng, H., Cruz, F.W., and Bouchaou, L., 2023, The spatiotemporal extent of the Green Sahara during the last glacial period. iScience 26.

Arenas, C., Auqué, L., Oscar, C., Sancho, C., Lozano, M. V., Vazquez-Urbez, M., Pardo, G., 2015, Current tufa sedimentation in a high discharge river: A comparison with other synchronous tufa records in the Iberian Range (Spain), Sedimentary Geology, 325, 132–157.

Arenas, C., Osacar, C., Sancho, C., Vazquer-Urbez, M., Auqué, L., Pardo, G., 2010, Seasonal record from recent fluvial Tufa deposits (Monasterio de Piedra, NE Spain): Sedimentological and stable isotope data. In M. Pedley, & M. Rogerson (Eds.), Tufas and speleothems: Unravelling the microbial physical controls, Geological Society, London, Special Publications, 336, 119–142.

Ashley, G.M., 2007, Orbital rhythms, monsoons and playa lake response, Olduvai Basin, equatorial East Africa (ca. 1.85-1.74 Ma), Geology, 35, 1091-1094.

Auqué, L., Arenas, C., Osacar, C., Pardo, G., Sancho, C., Vazquez-Urbez, M., 2014, Current tufa sedimentation in a changing- slope valley: The River Anamaza (Iberian Range, NE Spain), Sedimentary Geology, 303, 26–48.

Azennoud, K., Baali, A., Ait Brahim, Y., Ahouach, Y., Hakam, O., 2022, Climate controls o tufa deposition over the last 5000 years: A case study from Northwest Africa, Palaeogeography, Palaeoclimatology, Palaeoecology, 586, 110767.

Banerjee, D., Murray, A.S., Bøtter-Jensen, L., Lang, A., 2001, Equivalent dose estimation using a single aliquot of polymineral fine grains, Radiation Measurements 33, 73-94.

Bard, E., 2013, Out of the African Humid Period, Science, 342, 808-809.

Bergström, A., Stringer, C., Hajdinjak, M., Scerri, E. M. L., and Skoglund, P., 2021, Origins of Modern Human Ancestry, Nature, 590, 229–237.

Bøtter-Jensen, L., Thomsen, K.J., Jain, M., 2010, Review of optically stimulated luminescence (OSL) instrumental developments for retrospective dosimetry, Radiation Measurements 45, 253–257.

Brooke, I.A., 1993, Geomorphology and Quaternary Geology of the Dakhla Oasis region, Egypt, Quaternary Science Reviews, 12, 529-552.

Buylaert, J.P., Jain, M., Murray, A.S., Thomsen, K.J., Thiel, C., Sohbati, R., 2012, A robust feldspar luminescence dating method for Middle and Late Pleistocene sediments. Boreas 41, 435-451.

Channell, J.E.T., Hodell, D.A., Romero, O., Hillaire-Marcel, C., de Vernal, A., Stoner, J.S., Mazaud, A., Roehl, U., 2012, A 750-kyr detrital-layer stratigraphy for the North Atlantic (IODP sites U1302-U1303, Orphan Knoll, Labrador Sea), Earth Planet. Sci. Lett. 317, 218–230.

Chamley, H., 1989, Clay sedimentology. Springer, Heidelberg, 623 p.

Cheng H., Edwards R. L., Shen C.-C., Polyak V. J., Asmerom Y., Woodhead J., Hellstrom J., Wang Y., Kong X., Spötl C., Wang X. and Calvin E. C. A., 2013, Improvements in 230Th dating, 230Th and 234U half-life values, and U–Th isotopic measurements by multi-collector inductively coupled plasma mass spectrometry, Earth Planetary Science Letters, 371–372, 82–91.

Dalibard, M., Popescu, S.-M., Maley, J., Baudin, F., Melinte-Dobrinescu, M.-C., Pittet, B., Marsset, T., Dennielou, B., Droz, L., Suc, J.-P., 2014, High-resolution vegetation history of West Africa during the last 145 ka, Geobios 47, 183–198.

deMenocal, P., Ortiz, J., Guilderson, T., Adkins, J., Sarnthein, M., Baker, L., and Yarusinsky, M., 2000, Abrupt onset and termination of the African Humid Period: rapid climate responses to gradual insolation forcing, Quaternary Science Reviews, 19, 347-361.

Diffenbaugh, N.S., Giorgi, F., 2012, Climate change hotspots in the CMIP5 global climate model ensemble, Climatic Change, 114, 813-822.

Drake, N.A., El-Hawat, A.S., Turner, P., Armitage, S.J., Salem, M.J., White, K.H., McLaren, S., 2008, Palaeohydrology of the fazzan basin and surrounding regions: the last 7 million years. Palaeogeography, Palaeoclimatology, Palaeoecology, 263, 131-145.

Drake, N.A., Candy, I., Breeze, P., Armitage, S.J., Gasmi, N., Schwenninger, J.L., Peat, D., Manning, K., 2022, Sedimentary and geomorphic evidence of Saharan megalakes: A synthesis, Quaternary Science Reviews, 276, 107318.

Ehrmann, W., Schmiedl, G., Seidel, M., Krüger, S., Schulz, H., 2016, A distal 140 kyr sediment record of Nile discharge and East African monsoon variability, Climate of the Past, 12, 713-727.

Foerster, V., Deocampo, D.M., Asrat, A., Günter, C. Junginger, A., Krämer, K.H., Stroncik, N.A., Trauth, M., 2018, Towards an understanding of climate proxy formation in the Chew Bahir basin, southern Ethiopian Rift, Palaeogeography, Palaeoclimatology, Palaeoecology 501, 111–123.

Foerster, V., Asrat, A., Bronk Ramsey, C., Brown, E.T., Chapot, M.S., Deino, A., Duesing, W., Grove, M., Hahn, A., Junginger, A., Kaboth-Bahr, S., Lane, C.S., Opitz, S., Noren, A., Roberts, H.M., Stockhecke, M., Tiedemann, R., Vidal, C.M., Vogelsang, R., Cohen, A., Lamb, H.F., Schaebitz, F., Trauth, M.H., 2022, Pleistocene climate variability in eastern Africa influenced hominin evolution, Nature Geoscience, 15, 805–811.

Galway-Witham, J., Cole, J., and Stringer, C., 2019, Aspects of Human Physical and Behavioural Evolution during the Last 1 Million Years, Journal of Quaternary Science, 34 (6), 355–378.

Garcin, Y., Melnick, D., Strecker, M.R., Olago, D., Tiercelin, J.J., 2012, East African mid-Holocene wet-dry transition recorded in palaeo-shorelines of Lake Turkana, northern Kenya Rift, Earth and Planetary Sciences Letters, 331-332, 322-334.

Giorgi, F., 2006, Climate change hot-spots, Geophysical Research Letters, 33(8): L08707.

Guérin, G., Mercier, N., Adamiec, G., 2011. Dose-rate conversion factors: update, Ancient TL 29, 5-8.

Grant, K.M., Rohling, E.J., Westerhold, T., Zabel, M., Heslop, D., Konijnendjik, T. and Lourens, L., 2017, A 3-million-year index for North African humidity/aridity and the implication of potential pan-African Humid perids, Quaternary Science Reviews, 171, 100-118.

Groucutt H. S., Petraglia M. D., Bailey G., Scerri E. M. L., Parton A., Clark-Balzan L., Jennings R. P., Lewis L., Blinkhorn J., Drake N. A., Breeze P. S., Inglis R. H., Devès M. H., Meredith-Williams M., Boivin N., Thomas M. G., Scally A., 2015, Rethinking the dispersal of Homo sapiens out of Africa, Evolutionnary Anthropology. Issues News Rev. 24, 149–164.

Heinrich, H., 1988, Origin and consequences of cyclic ice rafting in the northeast Atlantic Ocean during the past 130,000 years. Quaternary Research, 29, 142–152.

Huntley, D.J., Baril, M.R., 1997, The K content of the K-feldspars being measured in optical dating or in thermoluminescence dating, Ancient TL 15, 11-13.

Huntley, D.J., Hancock, R.G.V., 2001, The Rb contents of the K-feldspar grains being measured in optical dating, Ancient TL 19, 43–46

Junginger, A., Trauth, M.H., 2013, Hydrological constraints of paleo-Lake Suguta in the Northern Kenya Rift during the African Humid Period (15–5 ka BP). Global Planetary Changes, 111, 174–188.

Kinsley, C.W., Bradtmiller, L.I., McGee, D., Galgay, M., Stuut, J.B., Tjallingii, R., Winckler, G., deMenocal, P.B., 2021, Orbital-and Millenial-Scale Variability in Northwest African Dust Emissions Over the Past 67,000 years, Paleoceanography and Paleoclimatology, 37, e2020PA004137.

Kuhlmann, H., Meggers, H., Freudenthal, T., Wefer, G., 2004, The transition of the monsoonal and the N Atlantic climate system off NW Africa during the Holocene. Geophysical Research Letters, 31, L22204

Kutzbach J. E., Guan J., He F., Cohen A. S., Orland I. J. and Chen G. (2020) African climate response to orbital and glacial forcing in 140,000-y simulation with implications for early modern human environments, Proceeding National Academy of Science, 117, 2255–2264.

Larrasoana, J.C., Roberts, A.P., and Rohing, E.J., 2013, Dynamics of Green Sahara Periods and their role in Hominin Evolution, PLOS one, 8, e76514.

Laskar, J., Robutel, P., Joutel, F., Gastineau, M., Correia, A.C.M., and Levrard, B., 2004, A long term numerical solution for the insolation quantities of the Earth, Astron. Astrophys. 428, 261-285.

Li, B., Li, S., 2012. A reply to the comments by Thomsen et al. on "Luminescence dating of K-feldspar from sediments: A protocol without anomalous fading correction." Quaternary Geochronology 8, 49–51.

Ludwig K. R. and Titterington D. M., 1994, Calculation of 230Th /U isochrons, ages, and errors. Geochim. Cosmochim. Acta, 58, 5031–5042.

Menviel, L., Govin, A., Avenas, A., Meissner, K.J., Grant, K.M., Tzedakis, P.C., 2021, Drivers of the evolution and amplitude of African Humid Periods, Communications earth and environment, 2, 237.

Murray, A.S., Helsted, L.M., Autzen, M., Jain, M., Buylaert, J.P., 2018, Measurement of natural radioactivity: Calibration and performance of a high-resolution gamma spectrometry facility, Radiation Measurements, 120, 215-220.

Murray, A., Arnold, L.J., Buylaert, J-P., Guérin, G., Qin, J., Singhvi, A.K., Smedley, R., Thomsen, K.J., 2021, Optically stimulated luminescence dating using quartz, Nature Reviews Methods Primers, 1,1.

Nutz, A., Schuster, M., 2016, Stepwise drying of Lake Turkana at the end of the African Humid Period: A forced regression modulated by solar activity variations? Solid Earth, 7, 1609–1618.

Nutz, A., Schuster M., Boes X., Rubino J.-L. 2017. Orbitally-driven evolution of Lake Turkana (Turkana Depression, Kenya, EARS) between 1.95 and 1.72 Ma: A sequence stratigraphy perspective, Journal of African Earth Sciences, 125, 230–243.

Nutz, A., Kwiecien, O., Breitenbach, S.F.M., Cai, Y., Della Porta, G., Danisch, J., Kabiri, L., Bodin, S., 2019, Fluvio-lacustrine sedimentation in the Agadir-Tissint Feija (Anti-

Atlas), Morocco): A promising palaeoclimate archive for the last glacial cycle in northwest Africa, The Depositional Record, 5(2), 362-387.

Nutz, A., Schuster, M., Barboni, D., Gassier, G., Van Bocxlaer, B., Robin, C., Ragon, T., Ghienne, J.F., Rubino, J.L., 2020, Plio-Pleistocene sedimentation in West Turkana (Turkana Depression, Kenya, East African Rift System): Paleolake fluctuations, paleolandscapes and controlling factors, Earth Science Reviews, 211(2), 103415.

Olsen, J., Anderson, N.J., Knudsen, M.F., 2012, Variability of the North Atlantic Oscillation over the past 5,200 years, Nature Geoscience, 5, 808–812.

Revel, M., Ducassou, E., Grousset, F.E., Bernasconi, S.M., Migeon, S., Revillon, S., Mascle, J., Murat, A., Zaragosi, S., Bosch, D., 2010, 100,000 Years of African monsson variability recorded in sediments of the Nile margin, Quaternary Science Review, 29, 1342-1362.

Sancho, C., Arenas, G., Vazquez-Urbez, M., Pardo, G., Lozano, M.V., Pena-Monne, J.L., Hellstrom, J., Ortiz, J.E., Osacar, M.C., Auqué, L., Torres, T., 2015, Climatic implications of the Quaternary fluvial tufa record in the NE Iberian Peninsula over the last 500ka, Quaternary Research, 84, 398-414.

Schaëbitz, F., Asfawossen, A., Lamb, H.F., Cohen, A.S., Foerster, V., Duesing, W., Kaboth-Bahr, S., Opitz, S., Viehberg, F.A., Vogelsang, R., Dean, J., Leng, M.J., Junginger, A., Bronk Ramsey, C., Chapot, M.S., Deino, A., Lane, C.S., Roberts, H.M., Vidal, C., Tiedemann, R., Trauth, M., 2021, Hydroclimate changes in eastern Africa over the past 200,000 years may have influenced early human dispersal, Communications Earth and Environment, 2, 123.

Schuster, M., Roquin, C., Duringer, P., Brunet, M., Caugy, M., Fontugne, M., Mackaye, H.T., Vignaud, P., Ghienne, J.F., 2005, Holocene Lake Mega-Chad palaeoshorelines from space, Quaternary Science Reviews, 24, 1821-1827.

Seidenglanz, A., Prange, M., Varma, V., Schulz, M., 2012, Ocean temperature response to idealized Gleissberg and de Vries solar cycles in a comprehensive climate model, Geophysical Research Letters, 39, L22602.

Sha, L., Ait Brahim, Y., Wassenburg, J.A., Yin, J., Peros, M., Cruz, F.W., Cai, Y., Li, H., Du, W., Zhang, H., et al. (2019). How far north did the african monsoon fringe expand during the african humid period? Insights from southwest Moroccan speleothems. Geophys. Res. Lett. 46, 14093-14102.

Shanahan, T.M., McKay, N.P., Hughen, K.A., Overpeck, J.T., Otto-Bliesner, B., Heil, C.W., King, J., Scholz, C.A., Peck, J., 2015, The time-transgressive termination of the African Humid Period, Nature Geosciences, 8, 140-144.

Sohbati, R., Murray, A., Lindvold, L., Buylaert, J.-P., Jain, M., 2017, Optimization of laboratory illumination in optical dating, Quaternary Geochronology, 39, 105-111.

Stevens, T., Buylaert, J.-P., Thiel, C., Újvári, G., Yi, S., Murray, A.S., Frechen, M., Lu, H., 2018, Ice-volume-forced erosion of the Chinese Loess Plateau global Quaternary stratotype site, Nature Communications 9, 983.

Thorp, M., Glanville, P., Stokes, S. and Bailey, R., 2002, Preliminary optical and radiocarbon age determinations for Upper Pleistocene alluvial sediments in the southern Anti Atlas Mountains, Morocco, Compte Rendus Geoscience, 334, 903-908.

Tierney, J.E., Pausata, F.S.R., and deMenocal, P.B., 2017a, Rainfall regimes of the Green Sahara, Science Advances, 3, e1601503.

Tierney, J.E., deMenocal, P.B., Zander, P.D., 2017b, A climatic context for the out-of-Africa migration, Geology, 45(11), 1023-1026.

Tjallingii, R., Claussen, M., Stuut, J-B.W., Fohlmeister, J., Jahn, A., Bickert, T., Lamy, F. and Rohl, U., 2008, Coherent high- and low-latitude control of the northwest African hydrological balance, Nature Geosciences, 1, 670-675.

Vermeesch P., 2018, IsoplotR: A free and open toolbox for geochronology. Geoscience Frontiers, 9, 1479–1493.

Wagner, B., Vogel, H., Francke, A., Friedrich, T., Donders, T., Lacey, J.H., Leng, M.J., Regattieri, E., Sadori, L., Wilke, T., et al. (2019). Mediterranean winter rainfall in phase with African monsoons during the past 1.36 million years. Nature 573, 256-260.

Wassenburg, J.A., Dietrich, S., Fietzke, J., Fohlmeister, J., Jochum, K.P., Scholz, D., Richter, D.K., Sabaoui, A., Spotl, C., Lohmann, G., Andreae, M.O., Immenhauser, A., 2016, Reorganization of the North Atlantic Oscillation during early Holocene deglaciation, Nature Geosciences, 9, 602e605.

Weil-Accardo, J., Feuillet, N. Philibosian, B. Guihou, A. Jacques, E. Cabioch G., Anglade, A. Meriaux, A.-S., Deschamps, P., 2022, Interaction Between Climate and Tectonics in the Northern Lesser Antilles Inferred From the Last Interglacial Shoreline on Barbuda Island, Geochemistry, Geophysics, Geosystems 23, 5: e2021GC010045.

Weldeab, S., Lea, D.W., Schneider, R.R., Andersen, N., 2007, 155,000 Years of West African Monsoon and Ocean Thermal Evolution, Science, 316(5829), 1303.

Zhao, H., Li, S.-H., 2005, Internal dose rate to K-feldspar grains from radioactive elements other than potassium, Radiation Measurements 40, 84-93.

Zielhofer, Ch., Fletcher, W.J., Mischke, S., De Batist, M., Campbell, J.F.E., Joannin, S., Tjallingii, R., El Hamouti, N., Junginger, A., Stele, A., Bussman, J., Schneider, B., Lauer, T., Spitzer, K., Strupler, M., Brachert, T., Mikdad, A., 2017, Atlantic forcing of Western Mediterranean winter rain minima during the last 12,000 years, Quaternary Science Reviews, 157, 29-51.

Zielhofer, Ch., Köhler, A., Mischke, S., Benkaddour, A., Mikdad, A., Fletcher, W.J., 2019, Western Mediterranean hydro-climatic consequences of Holocene ice-rafted debris (Bond) events, Climate of the Past, 15, 463-475.

Declaration of interests

☒The authors declare that they have no known competing financial interests or personal relationships that could have appeared to influence the work reported in this paper.

☐The authors declare the following financial interests/personal relationships which may be considered as potential competing interests:

Highlight

- U/Th and OSL ages date the occurrence of paleolake Tissint to between ~60 and ~50 ka.
- African Humid Period related to a 60-ka-centered insolation peak derived from precession variation.
- Heinrich event 6 (~60 ka) delayed the onset of humidification in northwest Africa.
- Heinrich event 5a (~55 ka) triggered short-term aridification in northwest Africa within the 60-50 ka humid interval.
- The 60-50 ka AHP may have facilitated the 60 ka human dispersal out of Africa.

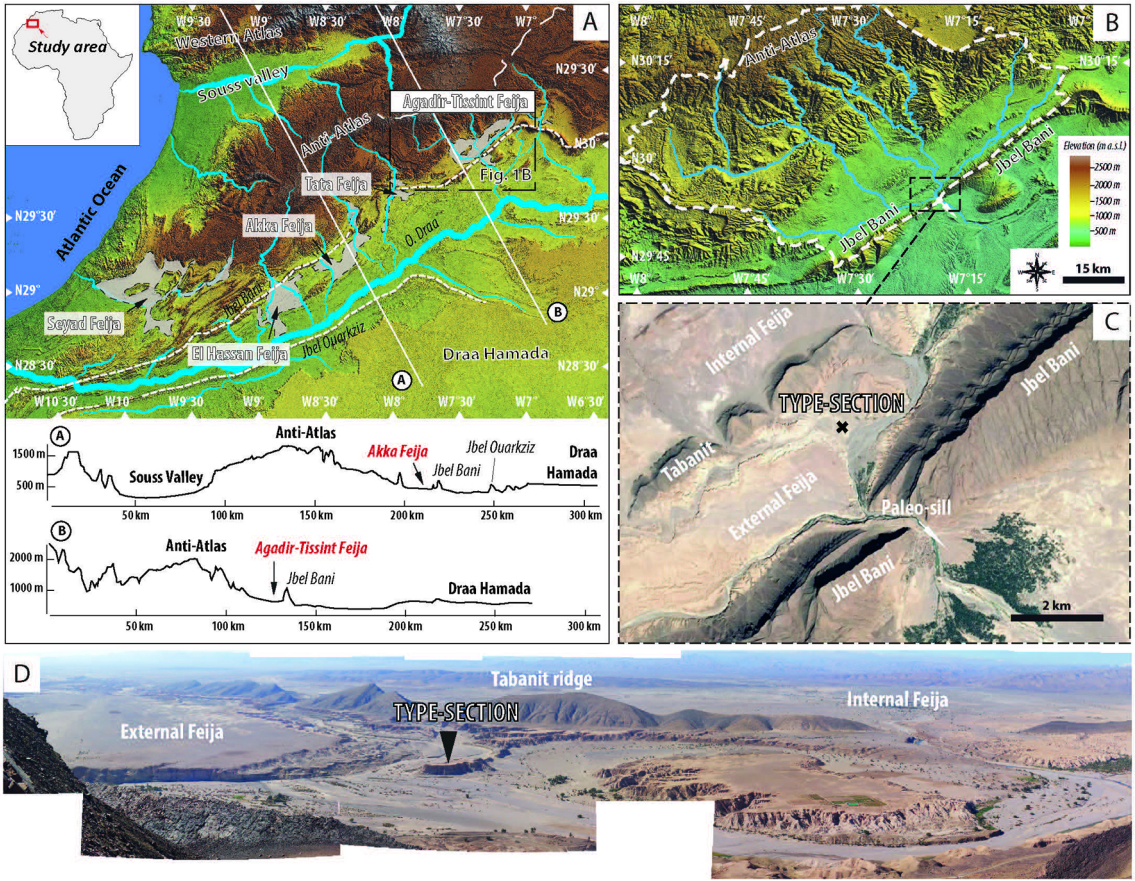
Study area
Western Atlas
Souss valley
Anti-Atlas
Agadir-Tissint Feija
Tata Feija
Akka Feija
Fig. 1B
Atlantic Ocean
O. Draa
Jbel Bani
Seyad Feija
El Hassan Feija
Jbel Ouarkziz
Draa Hamada
A
B
W9°30
W9°
W8°30
W8°
W7°30
W7°
N29°30
N30°
N29°
N28°30
W10°30
W10°
W9°30
W9°
W8°30
W8°
W7°30
W7°
W6°30
Anti-Atlas
Souss Valley
Akka Feija
Jbel Bani
Jbel Ouarkziz
Draa Hamada
1500 m
500 m
50 km
100 km
150 km
200 km
250 km
300 km
Anti-Atlas
Agadir-Tissint Feija
Jbel Bani
Draa Hamada
2000 m
1000 m
W8°
W7°45
W7°30
W7°15
W7°
N30°15
N30°
N29°45
Anti-Atlas
Jbel Bani
Elevation (in a.s.l.)
2500 m
2000 m
1500 m
1000 m
500 m
15 km
C
Internal Feija
Jbel Bani
TYPE-SECTION
Tabanit
External Feija
Paléo-sill
Jbel Bani
2 km
D
Tabanit ridge
TYPE-SECTION
External Feija
Internal Feija

Figure 1

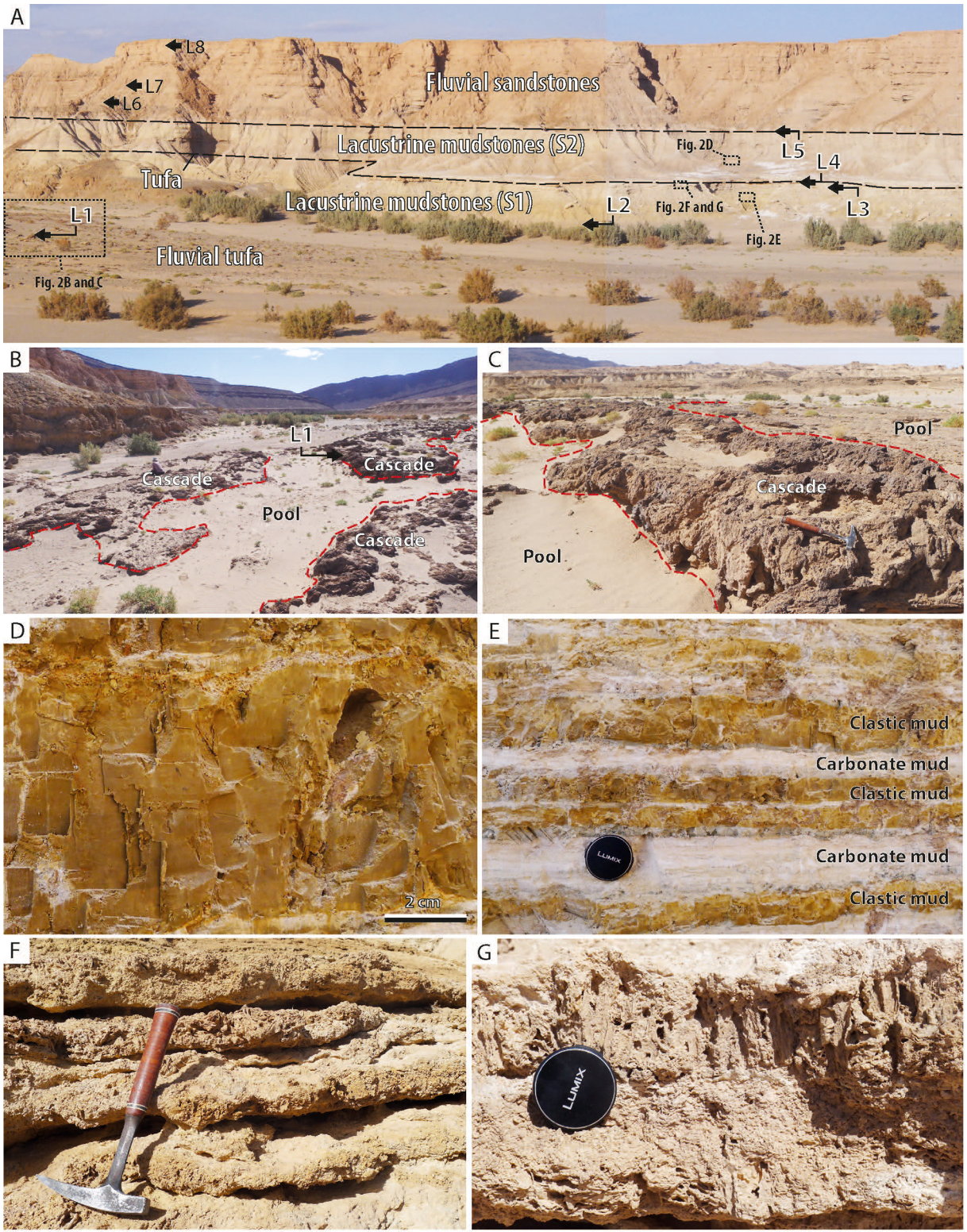
A
L8
L7
L6
Fluvial sandstones
Lacustrine mudstones (S2)
Fig. 2D
L5
L4
Tufa
Lacustrine mudstones (S1)
L2
Fig. 2F and G
L3
L1
Fig. 2E
Fluvial tufa
Fig. 2B and C
B
L1
Cascade
Cascade
Pool
Cascade
C
Pool
Cascade
Pool
D
2 cm
E
Clastic mud
Carbonate mud
Clastic mud
Carbonate mud
Clastic mud
F
G

Figure 2

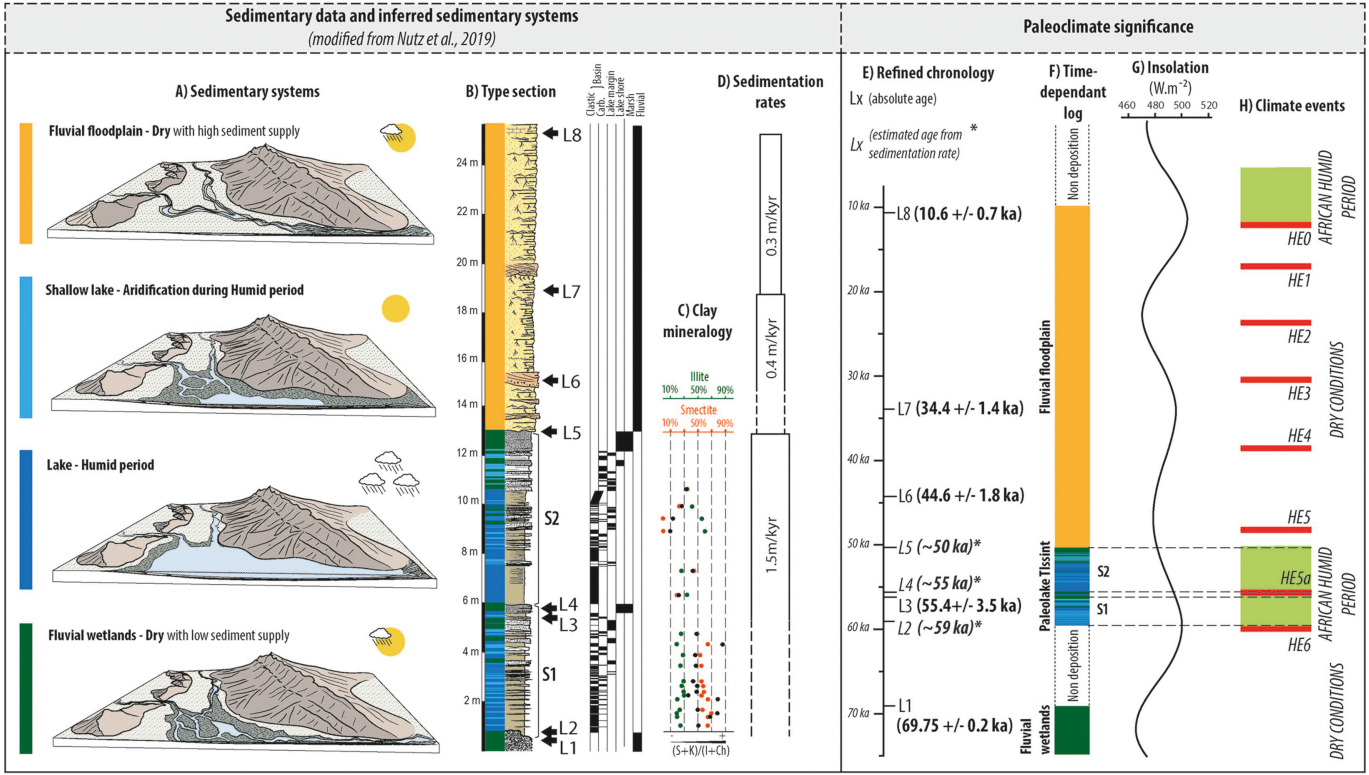
Sedimentary data and inferred sedimentary systems
(modified from Nutz et al., 2019)
Paleoclimate significance
A) Sedimentary systems
Fluvial floodplain - Dry with high sediment supply
Shallow lake - Aridification during Humid period
Lake - Humid period
Fluvial wetlands - Dry with low sediment supply
B) Type section
Clastic
Carb.
Basin
Lake margin
Lake shore
Marsh
Fluvial
L8
L7
L6
L5
L4
L3
L2
L1
S2
S1
24 m
22 m
20 m
18 m
16 m
14 m
12 m
10 m
8 m
6 m
4 m
2 m
C) Clay mineralogy
Illite
10%
50%
90%
Smectite
(S+K)/(I+Ch)
D) Sedimentation rates
0.3 m/kyr
0.4 m/kyr
1.5m/kyr
E) Refined chronology
Lx (absolute age)
Lx (estimated age from sedimentation rate) *
10 ka
20 ka
30 ka
40 ka
50 ka
60 ka
70 ka
L8 (10.6 +/- 0.7 ka)
L7 (34.4 +/- 1.4 ka)
L6 (44.6 +/- 1.8 ka)
L5 (~50 ka)*
L4 (~55 ka)*
L3 (55.4+/- 3.5 ka)
L2 (~59 ka)*
L1 (69.75 +/- 0.2 ka)
F) Time-dependant log
Non deposition
Fluvial floodplain
Paleolake Tissint
S2
S1
Non deposition
Fluvial wetlands
G) Insolation (W.m-2)
460
480
500
520
H) Climate events
AFRICAN HUMID PERIOD
HE0
HE1
HE2
HE3
HE4
DRY CONDITIONS
HE5
HE5a
AFRICAN HUMID PERIOD
HE6
DRY CONDITIONS

Figure 3

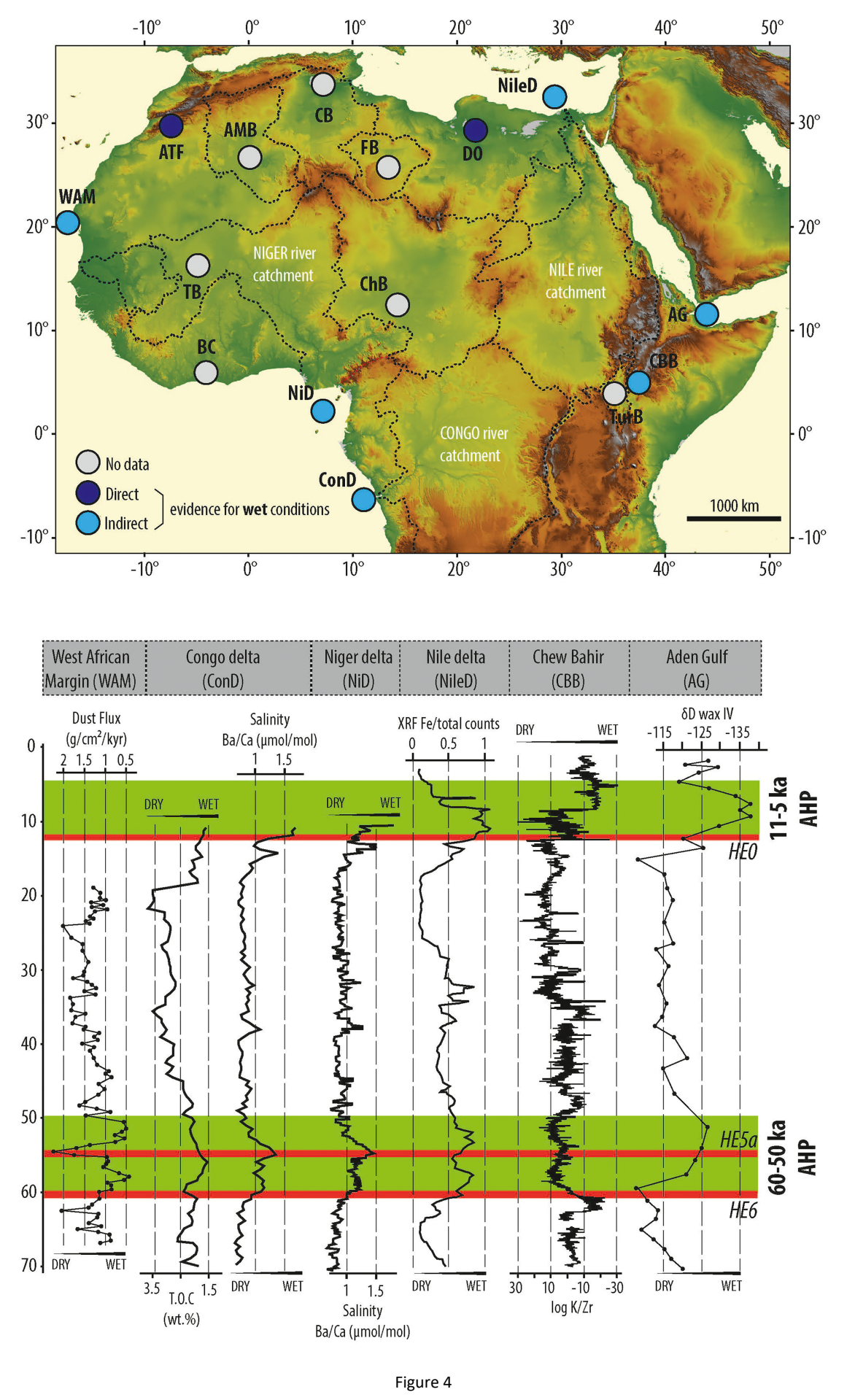
-10°
0°
10°
20°
30°
40°
50°
30°
20°
10°
0°
-10°
NileD
CB
ATF
AMB
FB
DO
WAM
NIGER river catchment
NILE river catchment
TB
ChB
AG
BC
CBB
NiD
T.urB
CONGO river catchment
ConD
No data
Direct
Indirect
evidence for wet conditions
1000 km
West African Margin (WAM)
Congo delta (ConD)
Niger delta (NiD)
Nile delta (NileD)
Chew Bahir (CBB)
Aden Gulf (AG)
Dust Flux (g/cm²/kyr)
Salinity Ba/Ca (µmol/mol)
XRF Fe/total counts
δD wax IV
DRY
WET
11-5 ka AHP
HE0
60-50 ka AHP
HE5a
HE6
T.O.C (wt.%)
log K/Zr

Figure 4